Electronegativity, susceptibility, and radiation shielding features of thulium reinforced barium-cadmium-lithium-borate glasses

B. M. Alotaibi[a], Thaqal M. Alhuzaymi[b], Mohammed. F. Alotiby[b], Sayed. A. Makhlouf[c], Kh. S. Shaaban[d], E. A. Abdel Wahab[c,*]
[a]*Physics Department, College of Science, Princess Nourah bint Abdulrahman University. P.O. Box 84428, Riyadh 11681, Saudi Arabia*
[b]*Nuclear Technologies Institute (NTI), King Abdulaziz City for Science & Technology (KACST), P. O. Box 6086, Riyadh, 11442, Saudi Arabia*
[c]*Physics Department, Faculty of Science, Al-Azhar University, Assiut, P.O 71524, Egypt*
[d]*Chemistry Department, Faculty of Science, Al-Azhar University, Assiut, P.O 71524, Egypt*

The chemical composition of the following glass system 75$Li_2B_4O_7$-10CdO-(15-x)BaO-$x$$Tm_2O_3$ ($0 \leq x \leq 2$) mol.% has been fabricated using a traditional melt quenching procedure. The density of the synthesis samples has been measured and it enhanced with the rising Tm_2O_3 content. All the fabricated specimens form glass and the amorphous state have been confirmed the XRD. The spectroscopic investigation indicates an increase in the energy gap from 3.08 to 3.25 eV with increasing Tm_2O_3 concentrations. The refractive index, basicity and static and infinity of dielectric constant were taken place of present investigated. The ultrasonic velocities of the prepared glasses are increased. Consequently, the elastic modulus of glasses has been enhanced. MCNP5, XCOM, and Phy-X/PSD code were used to characterize the efficiency of the fabricated glass against gamma radiation. Indeed, an increase in Tm_2O_3 content in samples correlated with an increase in MAC values. Consequently, the gamma-radiation attenuation rate of the samples was enhanced by the addition of Tm_2O_3, and the protective qualities were improved.

(Received May 14, 2024; Accepted August 2, 2024)

Keywords: Electronegativity, Susceptibility, Elastic modulus, MCNP5

1. Introduction

Glasses doped rare-earth ion (REI) like Er^{3+}, Tm^{3+}, Gd^{3+}, Sm^{3+} and Nd^{3+} are widely researched because of their enormous infrared laser applications [1-6]. Particularly, glasses doped Tm_2O_3 were extensively researched for application in advanced manufacturing [7]. Lithium-borate glasses are comparatively cheap and stable, with good mechanical characteristics [8-12]. Alkali and alkaline earth lithium-borate glasses including rare earth and transition metal oxides can dissolve huge amounts of various other oxide species [13-16].

Therefore, the presence of CdO in lithium-borate glasses as a glass modifier or an intermediate oxide provides numerous beneficial effects, such as doping with (REI) in an extensive variety, increasing chemical durability and strength to devitrification [17-18]. The introduction of BaO to the glass system Li_2O-B_2O_3-CdO increases the mechanical strength and makes it stable both in air and moisture conditions [19]. BaO and CdO incorporate glasses that have many particular aspects that are of significance to their applications, which are also used for the production of optical and radiation glasses [17-19]. Numerous scientists have developed $Li_2B_4O_7$ glasses that include BaO and CdO.

$Li_2B_4O_7$ - BaO - CdO - Tm_2O_3 glasses also attach great importance to their mechanical and radiation properties. The existence of Tm_2O_3 to $Li_2B_4O_7$ - BaO– CdO (BBLC) glasses plays an increasing role in broadening the characteristics of these glasses. (BBLC) glasses doped with Tm_2O_3 have greater applications across several regions, caused by chemical stability, low melting point, high density, excellent mechanical strength, shield protect radiation, and good

*Corresponding author: essam.ah77@gmail.com
https://doi.org/10.15251/CL.2024.218.583

transmission of FT-IR. The mechanical and radiation properties of the $Li_2B_4O_7$ - BaO - CdO - Tm_2O_3 glasses were discussed in this research paper. A pulse-echo procedure will be used for the estimation of the mechanical properties of these samples [20-25].

Different simulation and theoretical programs, such as MCNP5, XCOM, Phy-X/PSD, and Phy-X/Extra, can be used to calculate radiation shielding parameters. Monte Carlo simulations can be used to simulate a statistical process in theory (such as the interaction of photons or nuclear particles with materials).

For the fabricated glass system, optical, and mechanical measurements are investigated. MCNP5, XCOM, Phy-x/PSD, and Phy-X/Extra are used to characterize the shielding capability of the fabricated glasses against photons, fast neutrons and charged particles respectively.

Samples code:
$BBLC_0$: $0.75Li_2B_4O_7$+0.15BaO+0.1CdO;
$BBLC_{0.5}$: $0.75Li_2B_4O_7$+0.145BaO+0.1CdO+$0.005Tm_2O_3$;
$BBLC_1$: $0.75Li_2B_4O_7$+0.14BaO+0.1CdO+$0.01Tm_2O_3$;
$BBLC_{1.5}$: $0.75Li_2B_4O_7$+0.135BaO+0.1CdO+$0.015Tm_2O_3$ and
$BBLC_2$: $0.75Li_2B_4O_7$+0.13BaO+0.1CdO+$0.02Tm_2O_3$.

2. Materials and methods

The fabrication of the present glass samples can be found in Ref. [**2**]. The composition of $75Li_2B_4O_7$–(15–x) BaO–10CdO–xTm_2O_3, was used as listed in Table **1** with the following equation:

$$(Li_2CO_3+H_3BO_3)+BaO+CdO+Tm_2O_3 \xrightarrow[6H2O+CO2)]{\Delta\ at\ 600\ ^\circ C} [Li_2O+B_2O_3+BaO+Tm_2O_5+CdO] \xrightarrow{\Delta\ 1050\ ^\circ C} \text{glasses} \xrightarrow{annealing\ at\ 350\ ^\circ C} \text{glass samples.}$$

The densities (ρ) of the examined glasses were calculated using the Archimedes principle. Molar volume can be calculated using:

$$V_m = M/\rho. \tag{1}$$

The optical features were registered by Jasco 670 Instrument Japan. The transmission and absorption were recorded from 200 nm to 2000 nm.

Table 1. Chemical composition of BBLC glasses (mol %).

Sample name	Chemical Composition			
	$Li_2B_4O_7$	CdO	BaO	Tm_2O_3
$BBLC_0$	75	10	15	0
$BBLC_{0.5}$	75	10	14. 5	0. 5
$BBLC_1$	75	10	14	1
$BBLC_{1.5}$	75	10	13.5	1.5
$BBLC_2$	75	10	13	2

A pulse-echo procedure was examined (model 1085 of the KARL DEUTSCH Echograph) for mechanical measurements.

$$\text{longitudinal modulus, } L = \rho v_l^2, \tag{2}$$

$$\text{shear modulus, } G = \rho v_s^2, \tag{3}$$

$$\text{Young's modulus, } Y = (1+\sigma)2G \,, \tag{4}$$

$$\text{Bulk modulus, } K = L - \left(\frac{4}{3}\right) G \tag{5}$$

The theoretical calculation of the elastic moduli by dissociation energy and packing density [30,31] is as:

$$V_i = \left(\frac{3\pi}{4}\right) NA \{ m\mathrm{R}_{\mathrm{m}}^3 + n\,\mathrm{R}_{\mathrm{i}}^3 \} \tag{6}$$

$$\text{Poisson's ratio, } \sigma = \frac{1}{2} - \left(\frac{1}{7.2^*}\right) \tag{7}$$

$$\text{Micro Hardness } \mathrm{H} = \frac{(1-2\sigma)\mathrm{Y}}{6(1+\sigma)} \tag{8}$$

$$\text{Debye temperature, } \theta_D = \frac{h}{k}\left(\frac{9N}{4\pi\, V_m}\right)^{\frac{1}{3}} M_s \tag{9}$$

$$\text{Average of ultrasonic velocities } M_s = \frac{1}{3}\left(\frac{\frac{2}{v_T^3}}{\frac{1}{v_l^3}}\right)^{\frac{1}{3}} \tag{10}$$

$$\text{Thermal Expansion } \alpha_P = 23.2\,(v_L - 0.57457) \tag{11}$$

$$\text{Oxygen molar volume } V_o = \left(\frac{M}{\rho}\right)\left(\frac{1}{\sum xini}\right) \tag{12}$$

$$\text{Oxygen packing density } OPD = \left(\frac{1000\, C}{Vm}\right)\left(\frac{Mol}{L}\right) \tag{13}$$

The MPNC5 program software was used to simulate the value of the gamma intensity before and after the glass specimens. The XCOM program, on the other hand, is a user-friendly calculation that is based on near beam. The mass attenuation coefficient (μ/ρ) is the output of XCOM, while the sample composition is the input [26,27]. The Phy-X is a simple process for computing more than ten different parameters in a short time [28-29].

The gamma is attenuated when it passes through the absorbent material. The linear attenuation coefficient (LAC) is estimated by the Lambert-Beer [26]:

$$I = I_0\, e^{-\mu x} \tag{14}$$

whereI_o represents the measured γ-ray without the sample and I is the γ-ray intensity after the sample, and the sample thickness is x (cm). The mass attenuation coefficient (μ/ρ) estimated as:

$$\mu_{mass} = \mu/\rho \tag{15}$$

Radiation protection efficiency (RPE), is an important parameter for radiation protection and can be calculated by the following equation [27,28]:

$$\mathrm{RPE} = \left(1 - \frac{\mathrm{Io}}{\mathrm{I}}\right) \times 100 \text{ or } \mathrm{RPE} = (1 - \mathrm{FT}) \times 100, \text{ where } \mathrm{FT} = \frac{\mathrm{I}}{\mathrm{Io}}, \tag{16}$$

(TF) is the transmission factor.

Effective atomic number:

$$Z_{eff} = \sigma_a / \sigma_e, \tag{17}$$

Effective electron density:

$$N_{eff} = MAC/ \sigma_e \tag{18}$$

Total atomic cross-section:

$$\sigma_a = (1 / N_A) \sum f_i A_i (MAC)_I \tag{19}$$

Total molecular cross-section:

$$\sigma_m = (\mu/\rho) (M / N_A) , \ \sigma_m = (1 / N_A) \sum n_i A_i (MAC)_I, \tag{5}$$

Total electronic cross-section [29,30],

$$\sigma_e = (1 / N_A) \sum \frac{fi\,Ai}{Zi} (MAC)_I \tag{20}$$

where N_A is Avogadro's number.

Half and tenth value layers can be determined as:

$$HVL = 0.693 / \mu, \tag{21}$$

$$TVL = 2.303 / \mu \tag{22}$$

Mean free path:

$$MFP = 1/ \mu \tag{23}$$

These parameters are very important in radiation shielding [30, 31].

3. Results and discussion

3.1. Physical investigation

An XRD of the glass samples is exemplified in Fig. 1. It can be deduced that a high level of glassiness state, the presence of a small hill at 15 ~ 30°, and the absence of sharp peaks and discrete lines.

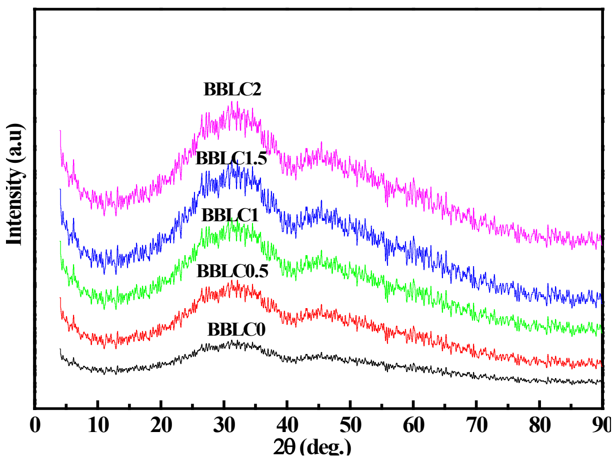

Fig. 1. XRD pattern of BBLC glasses doped Tm^{+3}.

There are two main reasons for increasing the density of our glass system. The first is the density difference between the two oxides BaO and Tm_2O_3 (5.72, 8.6), The second is the change in the mass of molecules, (153.326, 385.867) [32-36]. The values of correlation between both (ρ) and

V_m is listed in Table 2. It is seen the inverse proportionality between them. The oxygen molar volume of present glass has been computed and the values were written in Table 2. The oxygen packing density (OPD) was estimated and it is presented in Table 2. It is seen that that the OPD increase with increase Tm_2O_3 concentration.

Table 2. Structural characteristics of BBLC glasses.

Samples	$BBLC_0$	$BBLC_{0.5}$	$BBLC_1$	$BBLC_{1.5}$	$BBLC_2$
Glass Density (g/cm^3)	3.62	3.84	3.97	4.19	4.91
Glass molar volume (cm^3)	32.45	30.90	30.18	28.87	24.87
Oxygen molar volume (cm^3)	8.77	8.33	8.11	7.74	6.65
Oxygen packing density (OPD)	114.0	120.1	123.3	129.2	150.4
Ions conc. (N_i) (10^{21} ions/cm^3)	0	0.49	1.0	1.57	2.42
Inter-nuclear distance, r_i (Å)	0	12.7	10.0	8.61	7.44

3.2. Spectroscopic characteristic

The Spectrum of the fabricated glass samples is analyzed between 200 and 2000 nm. Tauc's plot is designed to obtain the optical band gap which measures the energy required to excite an electron from the valence band to the conduction band of a material. The optical band gap of the $75Li_2B_4O_7$- (15-x) BaO-10CdO-xTm_2O_3 ($0 \leq x \leq 2$) mol% glass system was increased from 3.08 eV to 3.25 eV [2] with rise thulium content as described in Table 3. The increase in band gap can be credited to the incorporation of Tm_2O_3 into the glass matrix. Tm_2O_3 is a trivalent lanthanide oxide with a relatively high electronegativity (2.207) [37]. This high electronegativity causes Tm_2O_3 to donate electrons to the glass network, leading to an increase in the average bond strength and a corresponding increase in the optical band gap. As a findings, the top energy of valance levels pushed down, which decreased the center of electron doner ln the network of glasses and can enhance the band gap [38]. A wider band gap indicates that the material is less transparent to visible light and more transparent to infrared light. This property makes Tm_2O_3-doped glasses attractive for applications such as infrared optical components. The following connection is used to estimate the retroactive index (n) of the fabricated sample as a function of the band gap energy: $n^2 = \sqrt{\frac{180}{E_g}} - 2$, and for other equations can be found in the bibliography as [39- 44].

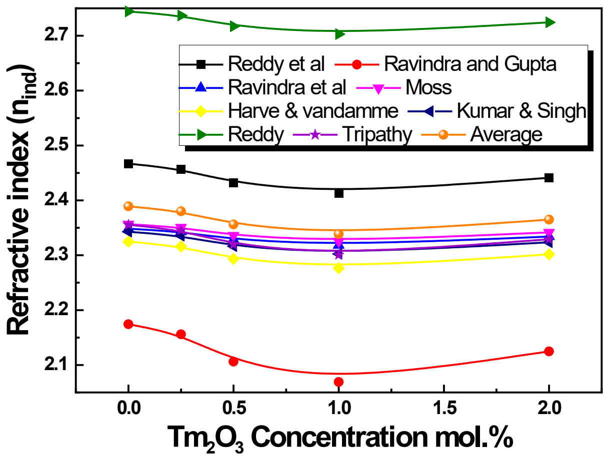

Fig. 2. Refractive index depending on indirect energy gap molar volume of BBLC glasses doped Tm^{+3}.

The refractive index decreases as the energy gap increases as ascribed in Fig. 2. So, the highest n of the fabricated glass sample is $BBLC_0$ and decreased with increased Tm_2O_3 concentration in the glass, which suggests that reducing in non-bridges oxygen formation. Other optical parameters have been estimated upon optical energy gap and refractive index as, R_L, α_m, α_o, $E_{e\text{-}ph}$, ε_o, ε_∞ and $\chi^{(1)}$, [45-51] their values are scheduled in Table 3. It is perceived that as the concentration of Tm^{+3} ions increase these parameters declined. This could be due to the creation of bridging oxygen in the glass matrix which leads to an increase in the ratio of BOs to NBOs. Also, Metallization criteria M, Basicity Λ, Transmission coefficient (T) and cohesive energy have been established. It is obvious that these parameters increase with rise the Tm^{+3} ions in the glass system. This could be because an increase in BOs in the glass system causes optical basicity to drop. Increased polarizability strengthens the capability of oxide ions to transport the negative charge. This shows that Tm0 has the highest ability to transfer electrons as compared to other glasses. As Tm_2O_3 concentration rises from 0 to 1.5 mol%, the values of other optical properties like nonlinear optical susceptibility ($\chi^{(3)}$) and nonlinear refractive index (n2) decrease. These variables have a direct relationship to the energy gap values and are explored in Fig. 3. The drop in non-bridging oxygen, which improves the energy band gap, could be the source of the declining behavior of these factors. The values recommend that the current glasses are an extremely effective option for non-linear applications of optical instruments [52].

Some parameters like optical energy gap, index refractions index, molar reflectivity Polarizability of cation (α_{cat}), Oxide ion polarizability(α_{O2-}), Molar Refractivity R_m (cm^3/mol), and Molar Polarizability α_m ($\mathring{A}^3$) have been designed theoretically from theoretical optical basicity. Their values are tabulated in Table 3. As can be seen, these factors in some cases follow the same trends but their magnitude differs from one factor to the other.

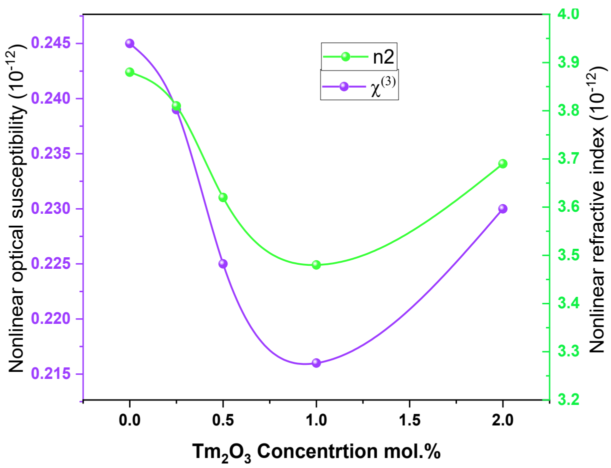

Fig. 3. Nonlinear optical susceptibility, refractive index of BBLC glasses doped Tm^{+3}.

Table 3. Various optical parameters of investigated glasses calculated based on optical bandgap.

Samples	$BBLC_0$	$BBLC_{0.5}$	$BBLC_1$	$BBLC_{1.5}$	$BBLC_2$
Oxygen packing density (OPD)	114.0	120.1	123.3	129.2	150.4
Indirect optical band gap (eV)	3.08	3.11	3.19	3.25	3.16
Refractive index ($n_{ind)}$ (average)	2.39	2.38	2.36	2.34	2.37
Molar Refractivity R_m (cm^3/mol)	1.504	1.505	1.507	1.509	1.511
Molar Polarizability α_m (A^{o3})	7.821	7.423	7.189	6.835	5.944
Metallization criterion (M)	0.392	0.394	0.399	0.403	0.397
Reflection loss (R_L)	0.166	0.165	0.162	0.160	0.163
Transmission coefficient (T)	0.715	0.717	0.721	0.724	0.719
Electronic polarizability(α_o)	2.755	2.748	2.728	2.714	2.736
Optical basicity (ʌ)	1.286	1.282	1.271	1.263	1.275
Steepness (S)	0.073	0.083	0.076	0.082	0.056
Electron phonon interaction (E_{e-ph})	9.16	8.00	8.72	8.18	11.91
Static refractive index n_o	2.38	2.37	2.35	2.33	2.36
Static dielectric constant ε_o	9.03	8.94	8.69	8.51	8.79
Infinity dielectric constant ε_∞	6.89	6.84	6.73	6.65	6.77
Linear dielectric susceptibility $\chi^{(1)}$	0.370	0.367	0.359	0.354	0.362
Nonlinear susceptibility $\chi^{(3)} \times 10^{-12}$ (esu)	0.245	0.239	0.225	0.216	0.23
$n_2 \times 10^{-12}$ (esu)	3.88	3.81	3.62	3.48	3.69
Cohesive energy CE(kcal/mol)	32.12	32.26	32.62	32.89	32.48
Cohesive energy CE(eV/atom)	1.40	1.41	1.42	1.44	1.42

3.3. Mechanical properties

The velocities of the glass samples were exemplified in Fig.4. With the rise in Tm_2O_3 content, both velocities are increased and represented in Table 4. [53-55]. Arrange the v_L between 4970, 5125m/s and v_T 2760, 2850 m/s. According to the previous FTIR analysis [2], the position of the band shifted to a higher wavenumber, which led to increased connectivity of the glass network.

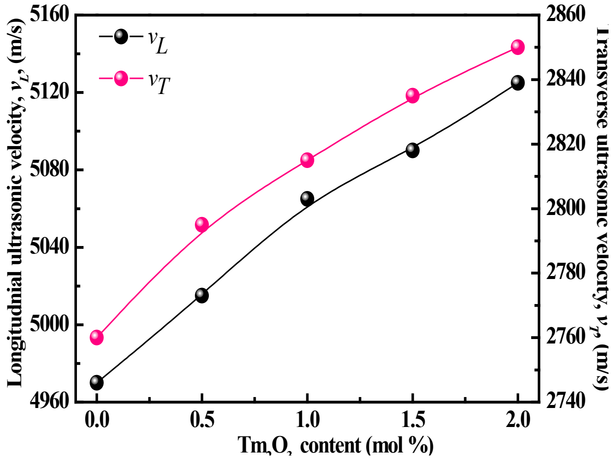

Fig. 4. v_L and v_T of BBLC glasses doped Tm^{+3}.

In Figs. 5&6 elastic moduli are exemplified with Tm_2O_3 content (experimentally and theoretically). Rising in the Tm_2O_3 content increases the elastic modulus values. This conduct is correlated to the change in the amount of coordination with the increase in Tm_2O_3 and the increase in average force and cross-link density. V_m reduces as Tm_2O_3 rises at the expense of BaO, and as the density rises, the glass structure becomes more compact. The conclusions of the data are represented in Table 5.

Table 4. Various optical parameters of investigated glasses calculated based on Theoretical optical basicity.

Samples	$BBLC_0$	$BBLC_{0.5}$	$BBLC_1$	$BBLC_{1.5}$	$BBLC_2$
Optical band gap (E_gth.) eV	5.23	4.70	4.43	3.96	2.50
Refractive index(n_{th})	1.97	2.05	2.09	2.18	2.547
Optical basicity (Λ_{th})	0.6075	0.6081	0.6087	0.6093	0.6099
Polarizability of cation (α_{cat})	0.0143	0.0145	0.0148	0.0153	0.0163
Oxide ion polarizability($\alpha_{O^{2-}}$)	1.572	1.573	1.574	1.574	1.575
Molar Refractivity R_m (cm^3/mol)	15.865	15.919	15.974	16.029	16.084
Molar Polarizability α_m (A^{o3})	6.296	6.317	6.339	6.361	6.382

Mechanical factors result (*Vi*), (*Gi*), (*H*), (α_P), (Z), (O_{PD}), (*Vo*), and (σ) are mentioned in Table 6. The glass network structure is correlated with this behavior. (*Vi*), (*H*), (α_P), (Z), (O_{PD}), (d), (*Gi*) and (σ) values are raised with an increase in the content of Tm_2O_3.

Table 5. The values of sound velocities (m/s), and elastic moduli(GPa) of BBLC glasses.

Sample name	V_L	V_T	L	G	K	Y	L_M	G_M	K_M	Y_M
$BBLC_0$	4970	2760	89.42	27.58	52.65	70.43	68.32	39.78	30.1	79.91
$BBLC_{0.5}$	5015	2795	96.58	30.00	56.58	76.48	72.19	44.25	31.4	86.12
$BBLC_1$	5065	2815	101.85	31.46	59.90	80.32	74.35	46.77	32.15	89.64
$BBLC_{1.5}$	5090	2835	108.55	33.68	63.65	85.88	78.16	51.58	33.44	96.16
$BBLC_2$	5125	2850	118.46	36.63	69.61	93.50	83.75	59.26	35.32	106.35

Table 6. The Values of, (Vi), (Gi), (α_P), (Z), and (θ_D), (O_{PD}), (V_o), (T_s) and, (H) of BBLC glasses.

Samples name	V_i $x10^{-6}$, (m^3)	Gi, (kcal/kJ)	α_p, (K^{-1})	d	σ	$Zx10^7$ (kg.m $^{-2}$.s^{-1})	θ_D, (K)	O_{PD}, (mol/L)	V_o, (cm^3/mol)	H, (GPa)	T_s, (°C)
$BBLC_0$	0.487	16.8	115290.67	2.1	0.2	1.80	364	114.011	8.784	4.1	602
$BBLC_{0.5}$	0.512	16.8	116334.67	2.1	0.2	1.93	376	120.752	8.269	4.51	620
$BBLC_1$	0.526	16.9	117494.67	2.1	0.2	2.01	382	124.638	8.027	4.69	631
$BBLC_{1.5}$	0.552	16.9	118074.67	2.1	0.2	2.13	391	130.621	7.657	5.05	645
$BBLC_2$	0.592	16.9	118886.67	2.1	0.3	2.31	401	138.110	7.246	5.47	661

V_o value is reduced due to the network of glass structures. The growth in rigidity in the glass structure is associated with an increase in the content of the network modifier (NWM).

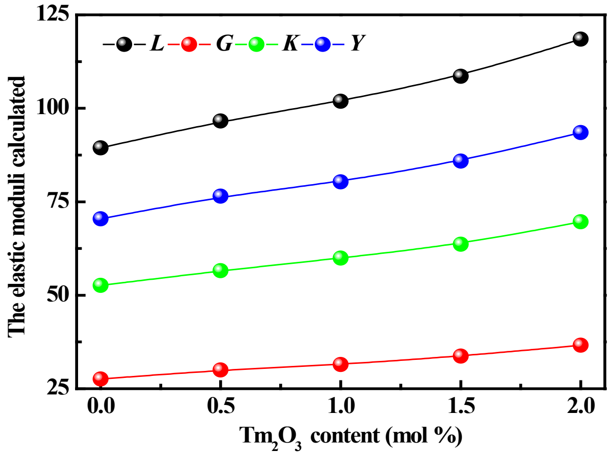

Fig. 5. Elastic moduli of BBLC glasses doped Tm^{+3}.

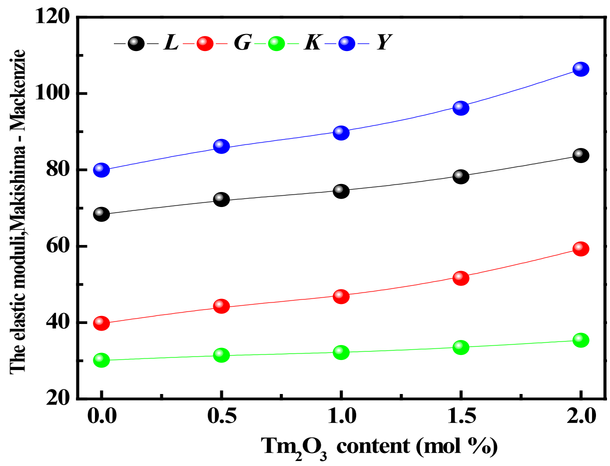

Fig. 6. Elastic moduli of BBLC glasses doped Tm^{+3}(Makishima – Mackenzie Model).

3.4 Radiation shielding calculation

The theoretical approach is a form of widespread method that uses some common equations to evaluate radiation shielding factors [56-58]. At the same time, we find some computer programs are now available to calculate these parameters for shielding in a short time and accurately, for example MCNP, Win X.com, Phy-X and Py-MLBUF [59-61]. In the present study, MCNP5, XCOM and Phy-X have been used to evaluate some radiation protection factors for the materials under investigation.

3.4.1. LAC and MAC

The LAC in (cm^{-1}) value has been calculated using the Beer-Lambert law at specified level of photon energy between (0.015MeV-15 MeV) [61]. The LAC value is the most important factor for calculating the radiation of glasses. Overall, the LAC is determined by the energy and density of the material under consideration. The density of the glass samples increases as the content of Tm_2O_3 increases. So, we note that the LAC depends on the concentration of Tm_2O_3 in the samples as illustrated in Fig. 7. It is seen the LAC for doped and undoped glasses have the same pattern with energy, whereas the concentration of Tm_2O_3 in the samples has the opposite tendency. Furthermore, the LAC declined dramatically at energies 0 to 0.04 MeV, decreased slowly at energies 0.04-0.4 MeV, and then practically stayed constant from 0.4 to 15 MeV.

Table 7 & Fig. 8 show MAC values acquired from (MCNP5, X.com and Phy-X/PSD) as well as the deviation (Rd %), which is calculated as $Rd = [(x - y)/x)100]$. The achieved findings have good agreement. Indeed, an increase in Tm_2O_3 content in samples correlated with an increase in MAC values. As a result, the inclusion of Tm_2O_3 enhances the attenuation rate of the glasses. The sample MACs show a similar LAC trend. As shown in Table **7**, these outcomes resemble the previously stated for other glass systems [10, 15, 16,18, 60]. The addition of Tm_2O_3 to the examined glasses, on the other hand, improves the protective qualities. In comparison to the other glass samples with glass examined in this study, the $BBLC_2$ had the highest value; thus, these glasses exhibited superior properties for radiation protection applications.

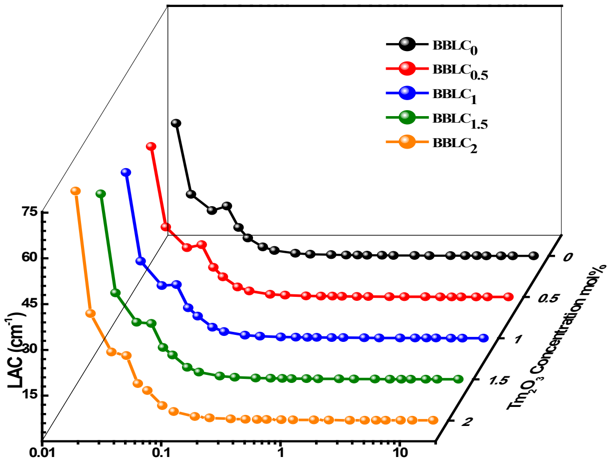

Fig. 7. The LAC variation of BBLC glasses doped Tm^{+3}.

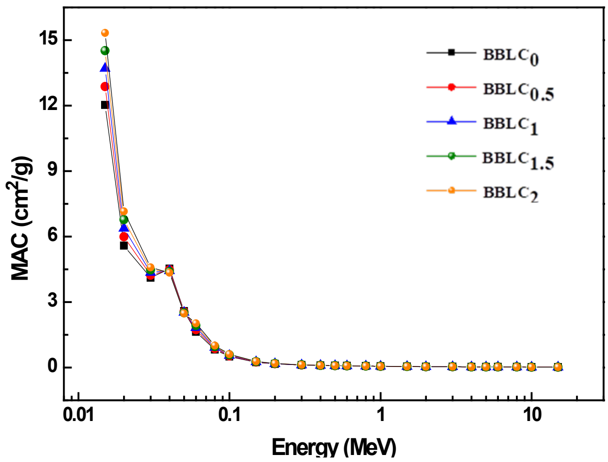

Fig. 9. Variation (MAC) of BBLC glasses doped Tm^{+3}.

3.4.2. (HVL) and MFP (λ)

Figures 10 and 11 show (HVL) and (MFP) of the prepared glasses. The values of (HVL) and (MFP) increase with photon energy (E). This information demonstrates that when the (E) increases, it gains the ability to penetrate the prepared sample on purpose. Increases in Tm_2O_3 cause decreases in (HVL) and (MFP) values as well. As a result, increasing Tm_2O_3 results in improved gamma radiation decrease. According to our statistics, $BBLC_2$ is the best sample. Because the highest value of HVL was at energy 15 MeV where it was 6.047 for $BBLC_2$ while it was 8.497 for $BBLC_0$. The achieved results were in good agreement [61]. The highest value of MFP was at energy 15 MeV was 8.725 for $BBLC_2$ while it was 12.259 for $BBLC_0$. The sample $BBLC_2$ has a lower value of (HVL) and (MFP) than the other samples, indicating that it is a better sample for shielding. As a result, we can conclude that increasing Tm_2O_3 improves radiation shielding. MFP and HVL exhibit the same trend as a result of the accurate simulation technique used for the examined sample.

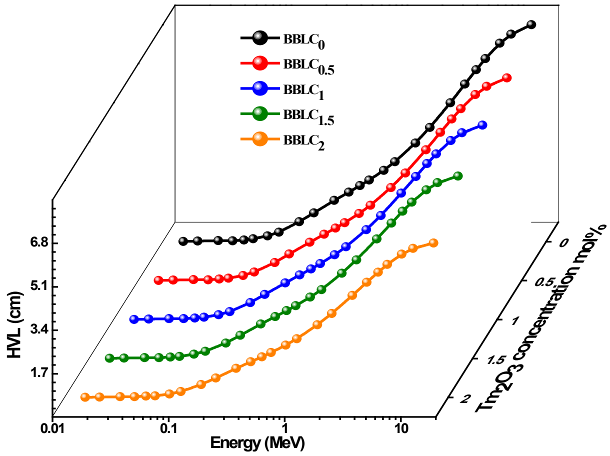

Fig. 10. The HVL of BBLC glasses doped Tm^{+3}.

3.4.3. Z_{eff}, Z_{eq} and electron N_e densities

The materials that have higher Z_{eff} or Ne values indicate a more effective shield [62]. Fig. 12(a&b) shows the change of the Z_{eff} and the Z_{eq} with energy, while Fig. 13 shows the change of the Ne with energy. The photoelectric absorption reactions are influenced by atomic number Z^4, Compton interactions are influenced by Z, and pair formation interactions are influenced by Z^2. The highest Z_{eff} value implies a better gamma-ray shield. So, we detected that the maximum values of the Z_{eff} are in the low energy (0 - 0.04) MeV, Where the photoelectric effect region. While it decreases with the increased energy as in Compton interactions region (0.04 – 1.5) MeV. On the other hand, the Z_{eff} increases in pair production interactions region with the increased energy (1.5 - 15) MeV, but it is still smaller than that in the photoelectric effect region. Another material property is the Z_{eq}, which can be seen in Fig. 13. Due to the Compton scattering, the (Z_{eq}) value increases as the energy increases, and it is small in the pair formation interactions region. The highest (Z_{eq}) value in the studied samples was 1.0 MeV. As the pair production interacts, the (Z_{eq}) value declines at energies higher than 1.0 MeV. The (Z_{eq}) value also rises as the amount of Tm_2O_3 in the samples rises. Generally, the Z_{eff} rises with an increase in Z, and with the increased concentration of Tm_2O_3 in samples.

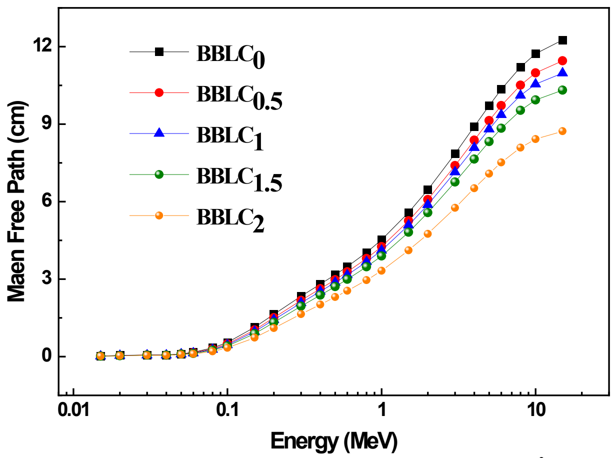

Fig. 11. (MFP) of BBLC glasses doped Tm^{+3}.

Therefore, we note that the highest value of the Z_{eff} is in the sample $BBLC_5$ which doped 2% Tm_2O_3 while the lowest value of the Z_{eff} is in the sample $BBLC_1$ which doped 0% Tm_2O_3. At the same time, it is seen that the change in the N_e with the increased energy has the same manner as the Z_{eff}, but the change in N_e was more affected than the change in Z_{eff}. So, the Ne was more evident than the Z_{eff} in a diagram as Illustrated in Figs. 12 a and 13.

3.4.4. (RPE) and (TF)

The RPE for the studied samples was calculated assuming that the glass thickness was 1.0 cm. From Table. 8 it is noted that the change in the (RPE) with the increased energy has the same behavior as the LAC. It is seen that the (RPE) values decrease with the increased energy. The high value of the (RPE) is noted at 0.255 MeV. This confirms that the studied samples are a good shielding they can be safe from radiation at the energy 0.255 MeV.

3.4.5. Effective Atomic Numbers Z_{eff} on protons, electrons, alpha particles, and C ions

The charged particles when falling on material, interact with the nuclei of that material. However, this interaction may be ignored as a means for energy loss because the probability of collision with nuclei is less than the probability of collision with electrons. So, the main interaction is a collision with electrons. Accordingly, the increase of the atomic numbers for glasses leads to an increase in the collision with electrons and leads to an increase in the collision-stopping power for the charged particles by materials. It is seen that the Z_{eff} values of both proton, Alpha, and Electron have the same behaviors. So, Z_{eff} values increase with increased atomic numbers of a prepared glass and, with the increase in energy of these charged particles. It was observed that the Z_{eff} values augmented as the content of Tm_2O_3 in samples increased and the sample $BBLC_2$ has higher values of Z_{eff} for this charged particle. therefore, it is Better than all samples as shielding to protection from the proton, Alpha, and Electron as shown in Fig. 14. Z_{eff} value of C ions augmented as the content of Tm_2O_3 increased, but it suddenly increased at energy 1.2 MeV then it has gradually decreased with the Energy for all investigated samples as shown Fig. 14. This may be due to an increase in the probability of the interaction between the C ions and the nuclei of the samples because of the large size of the carbon nucleus.

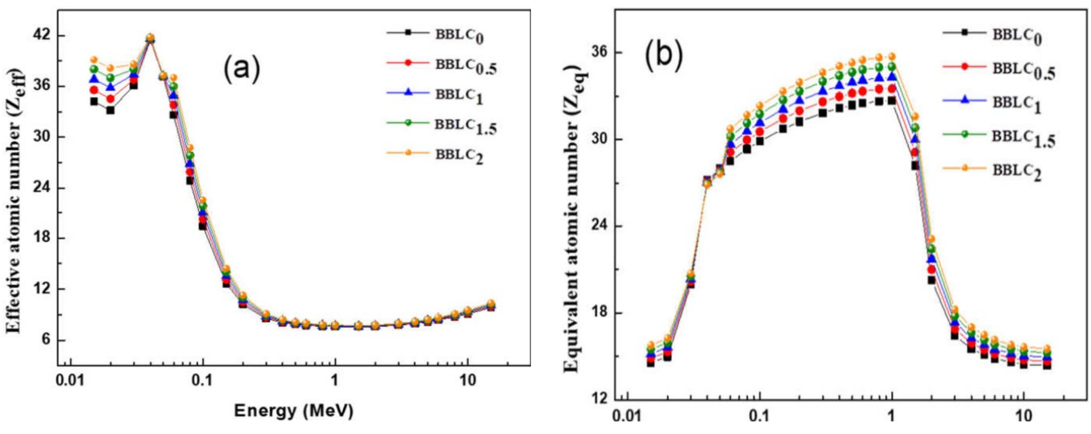

Fig. 12. The effective (a) and equivalent (b) atomic number of BBLC glasses doped Tm^{+3}.

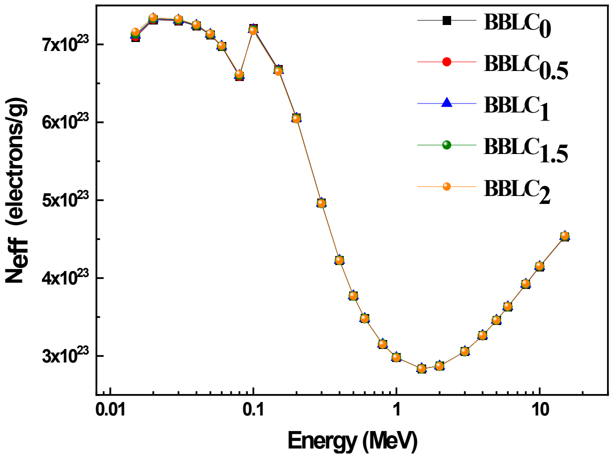

Fig. 13. N_{eff} of BBLC glasses doped Tm^{+3}.

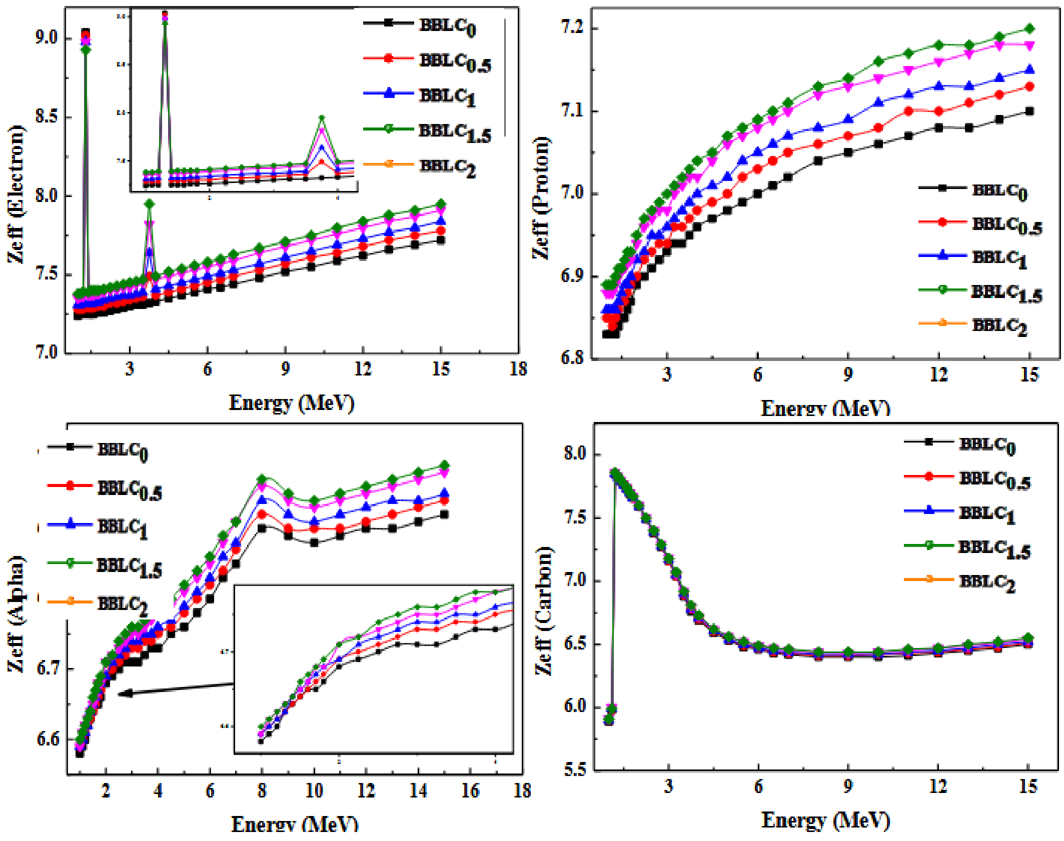

Fig. 14. Z_{eff} of Electron, Proton, Alpha and Carbon particles versus the energy of BBLC glasses doped Tm^{+3} ions.

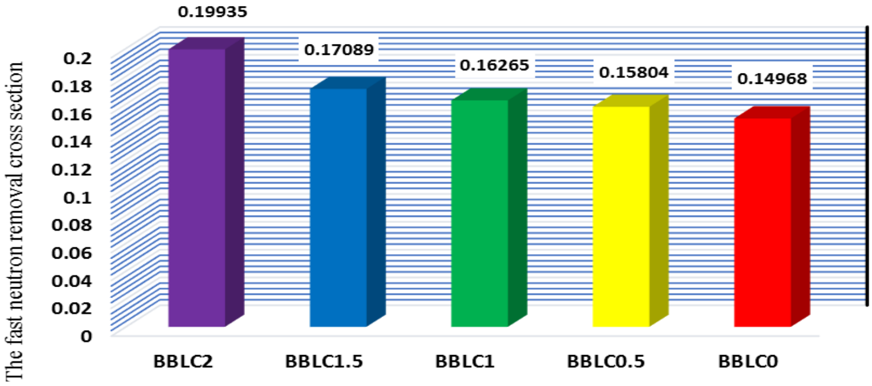

Fig. 15. The fast neutron removal cross-section of BBLC glasses doped Tm^{+3}.

3.4.6. Fast neutron attenuation coefficient, ΣR

Higher ΣR values lead to the materials having outstanding protection against opposite neutrons. In the present study, sample S5 had the highest ΣR value as shown in Fig. **15**, which had the biggest Percentage for Tm_2O_3 concentration 2%.

Table 7. Comparison of (MAC) calculated by using XCOM, MCNP5 and Phy-X BBLC glasses.

	$BBLC_0$				
Energy	MAC from XCOM	MAC from MCNP5	Dev% XCOM&MCNP	MAC from Phy-x/PSD	Dev% XCOM& Phy-x/PSD
0.015	1.33E+01	13.24357	0.048496	0.048496	0.307
0.02	6.15E+00	6.095886	-0.90412	-0.90412	0.279
0.03	4.87E+00	4.803607	-1.46542	-1.46542	0.279
0.04	5.04E+00	4.95161	-1.72449	-1.72449	0.315
0.05	2.86E+00	2.826013	-1.23803	-1.23803	0.275
0.06	1.81E+00	1.797008	-0.5004	-0.5004	0.213
0.08	8.98E-01	0.900643	0.304615	0.304615	0.054
0.1	5.44E-01	0.544543	0.026232	0.026232	0.000
0.15	2.57E-01	0.252152	-1.72436	-1.72436	0.146
0.2	1.74E-01	0.177371	1.787677	1.787677	0.162
0.3	1.20E-01	0.120033	0.110644	0.110644	-0.189
0.356 (0.992)*	1.07E-01	0.106554	0.050418	0.050418	-0.111
0.4	9.91E-02	0.100331	1.216659	1.216659	0.382
0.5	8.74E-02	0.088838	1.675351	1.675351	0.012
0.6	7.93E-02	0.080276	1.203584	1.203584	0.604
0.662 (0.0751)*	7.54E-02	0.075608	0.315264	0.315264	0.092
0.8	6.84E-02	0.068645	0.327882	0.327882	-0.358
1	6.10E-02	0.061476	0.741149	0.741149	-0.511
1.17 (0.0581)*	5.62E-02	0.056449	0.405511	0.405511	-0.069
1.33 (0.0551)*	5.26E-02	0.052891	0.587465	0.587465	0.552
1.5	4.94E-02	0.048819	-1.23029	-1.23029	0.078
2	4.27E-02	0.042056	-1.62721	-1.62721	-0.023
3	3.52E-02	0.035082	-0.451	-0.451	-0.699
4	3.12E-02	0.031223	0.17016	0.17016	0.322
5	2.87E-02	0.028545	-0.40297	-0.40297	0.462
6	2.70E-02	0.026715	-1.0662	-1.0662	0.383
8	2.51E-02	0.025295	0.928273	0.928273	-1.868
10	2.41E-02	0.023864	-0.86354	-0.86354	0.452
15	2.32E-02	0.023004	-0.93932	-0.93932	1.865

*Represents the experimentally measured value of MAC at the same energy.

	BBLC0.5				
Energy	MAC from XCOM	MAC from MCNP5	Dev% XCOM&MCNP	MAC from Phy-x/PSD	Dev% XCOM& Phy-x/PSD
0.015	1.29E+01	1.28E+01	-0.617	12.869	0.242493
0.02	6.00E+00	5.91E+00	-1.500	5.987	0.205758
0.03	4.23E+00	4.16E+00	-1.633	4.234	-0.13852
0.04	4.48E+00	4.48E+00	0.017	4.480	0.059959
0.05	2.56E+00	2.59E+00	1.367	2.554	0.043135
0.06	1.74E+00	1.71E+00	-1.388	1.733	0.184917
0.08	8.70E-01	8.56E-01	-1.617	0.868	0.173569
0.1	5.30E-01	5.23E-01	-1.482	0.530	0.161591
0.15	2.53E-01	2.52E-01	-0.450	0.253	0.115179
0.2	1.73E-01	1.71E-01	-0.937	0.173	0.071782
0.3	1.20E-01	1.20E-01	0.501	0.120	0.000888
0.356(0.0974)*	1.07E-01	1.06E-01	-0.302		
0.4	9.91E-02	9.85E-02	-0.615	0.099	0.018716
0.5	8.74E-02	8.78E-02	0.368	0.087	0.012894
0.6	7.94E-02	7.81E-02	-1.711	0.079	0.011515
0.662 (0.0749)*	7.55E-02	7.48E-02	-0.976		
0.8	6.86E-02	6.94E-02	1.190	0.069	-0.00074
1	6.12E-02	6.10E-02	-0.242	0.061	0.001299
1.77 (0.0587)*	5.63E-02	5.60E-02	-0.606		
1.33 (0.0549)*	5.27E-02	5.25E-02	-0.405		
1.5	4.95E-02	4.92E-02	-0.552	0.050	-0.00582
2	4.28E-02	4.31E-02	0.765	0.043	0.007864
3	3.52E-02	3.47E-02	-1.368	0.035	-0.00874
4	3.11E-02	3.08E-02	-0.835	0.031	0.014066
5	2.85E-02	2.81E-02	-1.314	0.029	0.007569
6	2.68E-02	2.64E-02	-1.421	0.027	-0.0046
8	2.48E-02	2.49E-02	0.584	0.025	0.021334
10	2.37E-02	2.35E-02	-0.862	0.024	0.011677
15	2.28E-02	2.26E-02	-0.705	0.023	0.039541

*Represents the experimentally measured value of MAC at the same energy.

Table 7. Continued

BBLC1					
Energy	MAC from XCOM	MAC from MCNP5	Dev% XCOM&MCNP	MAC from Phy-x/PSD	Dev% XCOM& Phy-x/PSD
0.015	1.37E+01	1.35E+01	1.242901	13.700	-0.294
0.02	6.36E+00	6.29E+00	1.119108	6.381	-0.269
0.03	4.35E+00	4.30E+00	1.323754	4.354	-0.034
0.04	4.43E+00	4.37E+00	1.352678	4.436	-0.049
0.05	2.53E+00	2.49E+00	1.582629	2.529	-0.062
0.06	1.83E+00	1.80E+00	1.276279	1.830	-0.251
0.08	9.13E-01	8.99E-01	1.500685	0.915	-0.227
0.1	5.54E-01	5.50E-01	0.772571	0.556	-0.204
0.15	2.61E-01	2.60E-01	0.359895	0.261	-0.164
0.2	1.77E-01	1.76E-01	0.455495	0.177	-0.078
0.3	1.21E-01	1.22E-01	-0.57382	0.121	-0.052
0.356 (0.0992)*	1.07E-01	1.07E-01	0.437054		
0.4	9.97E-02	1.00E-01	-0.34253	0.100	-0.022
0.5	8.78E-02	8.68E-02	1.141807	0.088	-0.017
0.6	7.96E-02	7.95E-02	0.11267	0.080	-0.015

BBLC$_1$					
Energy	MAC from XCOM	MAC from MCNP5	Dev% XCOM&MCNP	MAC from Phy-x/PSD	Dev% XCOM& Phy-x/PSD
0.662 (0.0762)*	7.57E-02	7.56E-02	0.126911		
0.8	6.86E-02	6.88E-02	-0.21849	0.069	-0.005
1	6.12E-02	6.18E-02	-0.91956	0.061	-0.007
1.77 (0.0566)*	5.64E-02	5.66E-02	-0.38838		
1.33 (0.0540)*	5.27E-02	5.27E-02	0.102944		
1.5	4.95E-02	4.94E-02	0.221706	0.050	0.008
2	4.28E-02	4.29E-02	-0.08913	0.043	-0.012
3	3.53E-02	3.54E-02	-0.2834	0.035	-0.017
4	3.11E-02	3.08E-02	0.979565	0.031	-0.006
5	2.86E-02	2.85E-02	0.140132	0.029	-0.014
6	2.69E-02	2.67E-02	0.732048	0.027	-0.019
8	2.49E-02	2.52E-02	-1.22179	0.025	-0.031
10	2.39E-02	2.35E-02	1.417003	0.024	-0.018
15	2.29E-02	2.28E-02	0.724132	0.023	-0.065

*Represents the experimentally measured value of MAC at the same energy.

Table 7. Continued

			BBLC$_{1.5}$		
Energy	MAC from XCOM	MAC from MCNP5	Dev% XCOM&MCNP	MAC from Phy-x/PSD	Dev% XCOM& Phy-x/PSD
0.015	1.46E+01	1.45E+01	0.198	14.520	0.206642
0.02	6.79E+00	6.69E+00	1.419	6.770	0.21919
0.03	4.47E+00	4.42E+00	1.105	4.473	-0.05407
0.04	4.40E+00	4.34E+00	1.393	4.393	0.144213
0.05	2.51E+00	2.47E+00	1.695	2.504	0.13531
0.06	1.93E+00	1.90E+00	1.681	1.925	0.206911
0.08	9.62E-01	9.54E-01	0.818	0.961	0.18598
0.1	5.82E-01	5.80E-01	0.292	0.581	0.162641
0.15	2.70E-01	2.69E-01	0.700	0.270	0.139278
0.2	1.81E-01	1.78E-01	1.463	0.181	0.087845
0.3	1.22E-01	1.24E-01	-1.162	0.122	0.076133
0.356 (0.102)*	1.08E-01	1.07E-01	0.659		
0.4	1.00E-01	9.89E-02	1.562	0.100	0.046127
0.5	8.81E-02	8.75E-02	0.740	0.088	0.015084
0.6	7.98E	8.01E	-0.343	0.080	0.0003

			BBLC1.5		
Energy	MAC from XCOM	MAC from MCNP5	Dev% XCOM&MCNP	MAC from Phy-x/PSD	Dev% XCOM& Phy-x/PSD
	-02	-02			62
0.662 (0.0759)*	7.58E-02	7.61E-02	-0.365		
0.8	6.87E-02	6.85E-02	0.333	0.069	0.007948
1	6.12E-02	6.10E-02	0.409	0.061	0.002233
1.17 (0.0562)*	5.64E-02	5.61E-02	0.524		
1.33 (0.0542)*	5.27E-02	5.22E-02	0.926		
1.5	4.96E-02	4.94E-02	0.302	0.050	0.001976
2	4.28E-02	4.26E-02	0.447	0.043	-0.00785
3	3.53E-02	3.49E-02	1.250	0.035	0.005353
4	3.12E-02	3.08E-02	1.354	0.031	0.009487
5	2.87E-02	2.89E-02	-0.931	0.029	0.002744
6	2.70E-02	2.74E-02	-1.569	0.027	0.009793
8	2.50E-02	2.52E-02	-0.665	0.025	0.00465
10	2.40E-02	2.40E-02	0.359	0.024	0.044675
15	2.32E-02	2.29E-02	1.311	0.023	0.061471

*Represents the experimentally measured value of MAC at the same energy.

Table 7. Continued

			BBLC2		
Energy	MAC from XCOM	MAC from MCNP5	Dev% XCOM&MCNP	MAC from Phy-x/PSD	Dev% XCOM& Phy-x/PSD
0.015	1.53E+01	1.51E+01	1.578	15.328	-0.05474
0.02	7.15E+00	7.05E+00	1.403	7.154	-0.06622
0.03	4.60E+00	4.53E+00	1.471	4.591	0.115333
0.04	4.35E+00	4.28E+00	1.565	4.350	0.005643
0.05	2.48E+00	2.47E+00	0.538	2.479	0.000263
0.06	2.02E+00	2.00E+00	0.874	2.019	-0.0557
0.08	1.01E+00	1.00E+00	0.356	1.006	-0.08054
0.1	6.06E-01	6.09E-01	-0.444	0.606	-0.05315
0.15	2.79E-01	2.76E-01	1.018	0.279	-0.03546
0.2	1.85E-01	1.85E-01	-0.356	0.185	-0.04862
0.3	1.24E-01	1.23E-01	0.868	0.124	-0.0264
0.356 (0.102)*	1.09E-01	1.09E-01	-0.457		
0.4	1.01E-01	9.97E-02	1.238	0.101	0.032884
0.5	8.85E-02	8.80E-02	0.509	0.088	-0.00399
0.6	8.00E-02	7.95E-02	0.666	0.080	-0.00596
0.662	7.60E-02	7.63E-02	-0.491		100

			BBLC2		
Energy	MAC from XCOM	MAC from MCNP5	Dev% XCOM&MCNP	MAC from Phy-x/PSD	Dev% XCOM& Phy-x/PSD
(0.0759)*					
0.8	6.88E-02	6.97E-02	-1.242	0.069	-0.00673
1	6.13E-02	6.09E-02	0.660	0.061	-0.00394
1.17 (0.0562)*	5.64E-02	5.68E-02	-0.632		
1.33 (0.0542)*	5.28E-02	5.29E-02	-0.227		
1.5	4.96E-02	4.98E-02	-0.409	0.050	-0.00367
2	4.29E-02	4.25E-02	0.804	0.043	-0.00314
3	3.54E-02	3.51E-02	0.783	0.035	0.000737
4	3.13E-02	3.10E-02	0.772	0.031	-0.0044
5	2.88E-02	2.88E-02	-0.197	0.029	-0.01082
6	2.71E-02	2.76E-02	-1.672	0.027	0.006391
8	2.52E-02	2.52E-02	-0.293	0.025	0.007376
10	2.42E-02	2.39E-02	1.226	0.024	-0.00839
15	2.33E-02	2.31E-02	1.140	0.023	-0.01686

*Represents the experimentally measured value of MAC at the same energy.

Table 8. The radiation protection efficiency (RPE) for all samples.

			RPE		
Energy	**BBLC0**	**BBLC0.5**	**BBLC1**	**BBLC1.5**	**BBLC2**
0.015	99.17222	99.45065	99.59363	99.71028	99.91346
0.02	88.99379	99.12277	91.7853	93.10486	95.86663
0.03	82.42874	84.37625	85.6212	87.34302	91.20527
0.04	83.34539	99.99277	85.29433	86.37185	89.93708
0.05	64.04912	99.58822	66.28138	67.67202	73.24905
0.06	99.85043	99.90243	99.93003	99.95635	99.99037
0.08	96.16242	96.78883	97.2814	97.93294	99.01862
0.1	86.07167	87.57883	88.89326	90.54662	94.0251
0.15	59.85973	62.83287	64.42953	66.60817	72.55254
0.2	47.38044	48.67336	50.19959	51.96095	58.54462
0.3	35.24238	37.14199	38.24286	40.15712	44.64647
0.356 (0.992)*	32.00422	33.56073	34.48883	36.0241	41.18328
0.4	30.45506	31.54521	32.72472	33.72889	38.39717
0.5	27.50081	28.61568	29.09373	30.56233	34.88166
0.6	25.21851	25.9016	27.02853	28.42501	32.17905
0.662 (0.0751)*	23.94415	24.94252	25.87042	27.22231	31.14205

			RPE		
Energy	**$BBLC_0$**	**$BBLC_{0.5}$**	**$BBLC_1$**	**$BBLC_{1.5}$**	**$BBLC_2$**
0.8	22.00264	23.36297	23.85584	24.8913	28.89509
1	19.95184	20.8503	21.70756	22.50604	25.77957
1.17 (0.0581)*	18.48189	19.31911	20.08658	20.91054	24.28469
1.33 (0.0551)*	17.4251	18.22282	18.83506	19.62886	22.8254
1.5	16.19908	17.20279	17.78917	18.66677	21.64308
2	14.12191	15.24747	15.62917	16.34378	18.81359
3	11.92628	12.50562	13.10077	13.58604	15.80016
4	10.68741	11.19685	11.5448	12.10668	14.11531
5	9.817321	10.30193	10.75101	11.43522	13.18082
6	9.217976	9.726244	10.10917	10.88281	12.64792
8	8.75	9.233194	9.597202	10.05414	11.64871
10	8.276119	8.767606	9.011487	9.587388	11.06261
15	7.990117	8.484268	8.767765	9.19184	10.70805

*Represents the experimentally measured value of MAC at the same energy.

4. Conclusion

The glasses with chemical compositions $0.75Li_2B_4O_7$+0.13BaO+0.1CdO+ $0.02Tm_2O_3$ were fabricated using melt-quench traditional method. The density was evaluated, and there is a rising trend with supplying Tm_2O_3. The amorphous nature of the produced samples was verified using the XRD. The incorporation of Tm_2O_3 into the $Li_2B_4O_7$ -BaO-CdO glass matrix significantly improves its optical properties, particularly its transparency in the near infrared region. The spectroscopy analysis recommends that the current glasses are an extremely effective option for non-linear applications of optical instruments. Tm_2O_3 doping also enhances the glass's mechanical strength, toughness and elastic moduli making it more resistant to breakage. MCNP5, X.COM, and Phy-X reveal that the glass exhibits favorable radiation shielding properties, making it a promising candidate for applications in nuclear radiation protection, especially the $BBLC_2$. The comparative analysis of optical, mechanical, and MCNP simulation characteristics demonstrates the potential of Tm_2O_3-doped $Li_2B_4O_7$ -BaO-CdO glasses for a wide range of applications, including non-linear optical tools, and radiation shielding protection.

Acknowledgements

This research project was funded by the Deanship of Scientific Research, Princess Nourah bint Abdulrahman University, through the Program of Research Project Funding After Publication, grant No (44- PRFA-P- 54).

References

[1] Wang, Xin; Li, Kefeng; Yu, Chunlei; Chen, Danping; Hu, Lili, Journal of Luminescence, **147**, 341(2014); https://doi.org/10.1016/j.jlumin.2013.11.025
[2] El-Maaref, A. A., Wahab, E. A. A., Shaaban, K. S., Abdelawwad, M., Koubisy, M. S. I., Börcsök, J., Yousef, E. S., Spectrochimica Acta Part A: Molecular and Biomolecular Spectroscopy,**242**, 118774(2020); https://doi.org/10.1016/j.saa.2020.118774
[3] Shaaban, K., Abdel Wahab, E.A., El-Maaref, A.A. *et al.,* J Mater Sci: Mater Electron **31,** 4986(2020); https://doi.org/10.1007/s10854-020-03065-8
[4] El-Maaref, A. A., Badr, S., Shaaban, K. S., Wahab, E. A., &ElOkr, M. M., Journal of Rare Earths, **37**(3), 253(2019); https://doi.org/10.1016/j.jre.2018.06.006
[5] E.A. Abdel Wahab, A.A. El-Maaref, Kh.S. Shaaban, J. Börcsök, M. Abdelawwad, Optical Materials,**111**, 110638(2021); https://doi.org/10.1016/j.optmat.
[6] Saudi, H.A., Abd-Allah, W.M. & Shaaban, K.S., J Mater Sci: Mater Electron **31,** 6963(2020). https://doi.org/10.1007/s10854-020-03261-6
[7] Byoungjin So, Jiangbo She, Yicong Ding, Jinsuke Miyake, Taisuke Atsumi, Katsuhisa Tanaka, Lothar Wondraczek, Opt. Mater. Express **9,** 4348-(2019); https://doi.org/10.1364/OME.9.004348
[8] Shaaban, K.S., Abo-Naf, S.M. &Hassouna, M.E.M., Silicon **11,** 2421(2019); https://doi.org/10.1007/s12633-016-9519-4
[9] Shaaban, K. S., Abo-naf S. M., Abd Elnaeim, A. M., &Hassouna, M. E. M., Applied Physics A, **123**(6), (2017); https://doi.org/10.1007/s00339-017-1052-9
[10] Fayad, A.M., Shaaban, K.S., Abd-Allah, W.M. *et al.*, J Inorg. Organo. Met. Polym. **30,** 5042(2020); https://doi.org/10.1007/s10904-020-01641-3
[11] Shaaban, K.S., Wahab, E.A.A., Shaaban, E.R. et al., Journal of Elec Materi **49**, 2040(2020); https://doi.org/10.1007/s11664-019-07889-x
[12] Abd-Allah, W.M., Saudi, H.A., Shaaban, K.S. et al., Appl. Phys. A **125,** 275 (2019); https://doi.org/10.1007/s00339-019-2574-0
[13] E.A. Abdel Wahab,M.S.I. Koubisy, M.I. Sayyed, K.A. Mahmoud, A.F. Zatsepin,Sayed A. Makhlouf, Shaaban, Kh.S., Journal of Non-Crystalline Solids, **553**, 120509(2021), https://doi.org/10.1016/j.jnoncrysol.2020.120509
[14] Shaaban, K.S., Koubisy, M.S.I., Zahran, H.Y. et al., J Inorg. Organo. Met. Polym. **30,** 4999(2020); https://doi.org/10.1007/s10904-020-01640-4
[15] El-Sharkawy RM, Shaaban KS, Elsaman R, Allam EA, El-Taher A, Mahmoud ME, J Non-Cryst Solids **528**(15), 119754(2020); https://doi.org/10.1016/j.jnoncrysol.2020
[16] Abd-Allah, W.M., Saudi, H.A., Shaaban, K.S. et al, Appl. Phys. A **125,** 275(2019); https://doi.org/10.1007/s00339-019-2574-0
[17] Wahab, E. A. A., Shaaban, K. S., Materials Research Express, **5**(2), 025207(2018); https://doi.org/10.1088/2053-1591/aaaee8
[18] Shaaban, K.S., Wahab, E.A.A., Shaaban, E.R. et al. Opt Quant Electron **52,** 125(2020) ; https://doi.org/10.1007/s11082-020-2191-3
[19] Shaaban, K.S., Yousef, E.S., Mahmoud, S.A. et al. J Inorg. Organ. met. Polym.,(2020); https://doi.org/10.1007/s10904-020-01574-x
[20] Shaaban, K.S., Yousef, E.S., Abdel Wahab, E.A. *et al.,* J. of Materi. Eng and Perform **29,** 4549(2020); https://doi.org/10.1007/s11665-020-04969-6
[21] El-Rehim, A.F.A., Ali, A.M., Zahran, H.Y. et al., J. Inorg. Organo. Met. Polym. (2020); https://doi.org/10.1007/s10904-020-01799-w
[22] Abdel Wahab, E.A., Shaaban, K.S. Yousef, E.S., Opt Quant Electron **52**, 458(2020); https://doi.org/10.1007/s11082-020-02575-3
[23] K. Singh, L. Gerward, Indian Journal of Pure and Applied Physics, **40(**9), 643(2002).
[24] M.I. Sayyed, Ali A. Ati, M.H.A. Mhareb, K.A. Mahmoud, Kawa M. Kaky, S.O. Baki, M.A. Mahdi, Journal of alloys and compounds 155668(2020); https://doi.org/10.1016/j.jallcom.2020.155668.
[25] E. A. Abdel Wahab, Kh. S. Shaaban, Sultan Alomairy, M. S. Al-Buriahi, Eur. Phys. J. Plus **136**, 636(2021); https://doi.org/10.1140/epjp/s13360-021-01572-z

[26] Ö. F. Özpolat, B. Alım, E. Şakar, M. Büyükyıldız, M. Kurudirek, Radiation and Environmental Biophysics **59**, 321(2020); https://doi.org/10.1007/s00411-019-00829-7
[27] Alothman, M.A., Alrowaili, Z.A., Alzahrani, J.S., Wahab, E.A.A., Olarinoye, I.O., Sriwunkum, C., Shaaban, K.S., Al-Buriahi, M.S., Journal of Alloys and Compounds, **882**, 160625 (2021); https://doi.org/10.1016/j.jallcom.2021.160625
[28] S. R. Manohara, S. M. Hanagodimath, and L. Gerward, Medical Physics **l35**,1 388(2008).
[29] Makishima, A., J.D. Mackenzie, Journal of Non-Crystalline Solids, **12**(1), 35(1973); https://doi.org/10.1016/0022-3093(73)90053-7
[30] Makishima, A., J.D. Mackenzie, Journal of Non-crystalline solids, **17**(2), 147(1975); https://doi.org/10.1016/0022-3093(75)90047-2
[31] S. Gowda, S. Krishnaveni, and R. Gowda, Nuclear Instruments and Methods in Physics Research B: Beam Interactions with Materials and Atoms, **239**, 361(2005); https://doi.org/10.1016/j.nimb.2005.05.048
[32] Amal A. El-Sawy, International Journal of Hybrid Information Technology **9**, 437(2016).
[33] Kavaz E., Tekin H.O., Agar O., Altunsoy E.E., Kilicoglu O., Kamislioglu M., Abuzaid M.M., Sayyed M.I., Ceram. Int. **45**. (12), 15348(2019); https://doi.org/10.1016/j.ceramint.2019.05.028
[34] Xinyu Zhaoa, Xiaoli Wangb, Hai Lina, Zhiqiang Wang, Physica B **392** 132 (2007); https://doi.org/10.1016/j.physb.2006.11.015
[35] M. H. A. Mhareb, M. A. Almessiere, M. Sayyed, Y. Alajerami, Optik **182** 821(201); https://doi.org/10.1016/j.ijleo.2019.01.111
[36] M.V. Kurik, Urbach rule (Review), Wiley-VCH, Phys. Stat. Sol. (a), vol.8, pp.9-30, 1971 ; https://doi.org/10.1002/pssa.2210080102
[37] G.D. Cody, Urbach edge of crystalline and amorphous silicon: a personal review, Elsevier, J. Non-Cryst. Solids, **141,** 3 (1992); https://doi.org/10.1016/S0022-3093(05)80513-7
[38] Ihor Studenyak, Mladen Kranjčec, Mykhailo Kurik, **4**, (3), 76 (2014); https://doi.org/10.5923/j.optics.20140403.02
[39] Nagaraja, M., Raghu, P., Mahesh, H.M. Pattar J., J Mater Sci: Mater Electron **32**, 8976(2021); https://doi.org/10.1007/s10854-021-05568-4
[40] Wahab, E.A.A., Alyousef, H.A., El-Rehim, A.F.A., Shaaban, K.S., Journal of Electronic Materials, **52** (1), 219 (2023); https://doi.org/10.1007/s11664-022-09969-x
[41] Wahab, E.A.A., Shaaban, K.S., Al-Baradi, A.M., Silicon, **14** (9), 4915(2022); https://doi.org/10.1007/s12633-021-01236-8
[42] El-Rehim, A.F.A., Wahab, E.A.A., Halaka, M.M.A., Shaaban, K.S., Silicon, **14** (2) (2022) pp. 373-384; https://doi.org/10.1007/s12633-021-01002-w
[43] Yangang Liu, Peter H. Daum, Journal of Aerosol Science, **39**, (11), 974 (2008); https://doi.org/10.1016/j.jaerosci.2008.06.006
[44] W. Heller, Journal of Physical Chemistry, **69**, 1123(1965); https://doi.org/10.1021/j100888a006
[45] V. Dimitrov, S. Sakka. J Appl. Phys. **79**, 1741–1745 (1996); https://doi.org/10.1063/1.360963
[46] S. Adachi, Optical properties, properties of group-IV, III-V and II-VI semiconductors, Chichester, UK, John Wiley & Sons Ltd, 211–281(2005); https://doi.org/10.1002/0470090340.ch10
[47] A.H. Hammad, E.B. Moustafa, J. Non-Cryst. Solids **544**, 120209 (2020); https://doi.org/10.1016/j.jnoncrysol.2020.120209
[48] E.A.A. Wahab, Kh.S. Shaaban,. Appl. Phys. A **127**, 956 (2021); https://doi.org/10.1007/s00339-021-05062-y
[49] Wahab, EAA, Aboraia, AM, Shafey, AME, Shaaban, KS, Soldatov, AV, OPTICAL AND QUANTUM ELECTRONICS, **53**, 9 (2021); https://doi.org/10.1007/s11082-021-03164-8
[50] Somaily, H.H., Shaaban, K.S., Makhlouf, S.A. et al, J Inorg. Organo. met. Polym. (2020); https://doi.org/10.1007/s10904-020-01650-2
[51] Shaaban, K. S., El Sayed Yousef, Optik - International Journal for Light and Electron Optics **203**,163976(2020); https://doi.org/10.1016/j.ijleo.2019.163976
[52] Abdel Wahab, E.A., Shaaban, K.S., Elsaman, R. et al., Appl. Phys. A **125,** 869(2019); https://doi.org/10.1007/s00339-019-3166-8

[53] Wahab, E. A. A., Shaaban, Kh. S.. Materials Research Express, **5**(2), 025207(2018); https://doi.org/10.1088/2053-1591/aaaee8
[54] Al-Hadeethi Y, Sayyed MI, Rammah YS., Ceram Int; **46** (2055), 62(2020); https://doi.org/10.1016/j.ceramint.2019.09.185
[55] Al-Buriahi MS, Singh VP, J Aust. Ceram. Soc;**1**–7(2020).
[56] Yasmin S, Barua BS, Khandaker MU, Rashid MA, Bradley DA, Olatunji MA, et al. Results Phys; **9**(541),9(2018); https://doi.org/10.1016/j.rinp.2018.02.075
[57] Gerward L, Guilbert N, Jensen KB, Levring H, Radiat Phys Chem;**71**:653(2004); https://doi.org/10.1016/j.radphyschem.2004.04.040
[58] Mann Kulwinder Singh, Mann Sukhmanjit Singh. Ann Nucl Energy; **150**:107845(2021).
[59] Mirji R, Lobo B. Radiat Phys Chem; **135**:32(2017); https://doi.org/10.1016/j.radphyschem.2017.03.001.
[60] S. Kaur, A. Kaur, P.S. Singh, T. Singh, Prog. Nucl. Energy **93**, 277(2016); https://doi.org/10.1016/j.pnucene.2016.08.022
[61] K. Singh, H. Singh, V. Sharma et al., Nuclear Instruments and Methods in Physics Research B: Beam Interactions with Materials and Atoms, **194**, 1(2002); https://doi.org/10.1016/S0168-583X(02)00498-6
[62] V.P. Singh, N.M. Badiger, Radiat. Phys. Chem. **104** 61(2014); https://doi.org/10.1016/j.radphyschem.2013.11.025.
[69] Y. Karabul, L. Amon Susam, O. Içelli, _ O. Eyecioglu, Nucl. Instrum. Methods Phys. Res. Sect. A Accel. Spectr. Detect. Assoc. Equip. **797**, 29(2015); https://doi.org/10.1016/j. nima.2015.06.024.